PROCEEDINGS, Thirty-Seventh Workshop on Geothermal Reservoir Engineering
Stanford University, Stanford, California, January 30 - February 1, 2012
SGP-TR-194

PRELIMINARY MODEL OF FRACTURE AND STRESS STATE IN THE HELLISHEIDI GEOTHERMAL FIELD, HENGILL VOLCANIC SYSTEM, ICELAND

Joseph Batir[1], Nicholas C. Davatzes[2] and Ragnar Asmundsson[3]

1) Southern Methodist University – Huffington Dept. of Earth Sciences, 3225 Daniel Ave, Dallas, TX 75275 (formerly at the School for Renewable Energy Science)
2) Temple University – 1901 N. 13th Street, Earth and Environmental Science, Beury Hall, Rm. 307, Philadelphia, PA, 19122
3) Iceland GeoSurvey (ISOR) – Rangarvollum, 603 Akureyri, Iceland (currently at Tiger Energy Services, New Zealand)

Corresponding author's e-mail: jbatir@smu.edu

ABSTRACT

A Borehole Televiewer (BHTV) image log of borehole HN-16 was acquired in October 2010 by the Iceland GeoSurvey (ISOR) to a total measured depth of 2,191 m in the Hellisheidi Geothermal Field, in SW Iceland. The HN-16 images reveal the attitude of natural fractures are strongly clustered with a mean true strike azimuth from ~220-230 and true dip from 71-78° that is consistent with the strike of rift-graben faults mapped at the surface which bound the geothermal field. This clustering appears independent of the borehole deviation direction, which is roughly due north in the imaged interval. Although the majority of these fractures are partially or fully healed, as inferred from minimal surface topography across the borehole wall, many appear to be open based on loss of signal in the image log and the higher injectivity of HN-16.

Structures resulting from drilling-induced borehole failure include petal-centerline fractures, some tensile fractures, and abundant breakouts (which were unexpected in a presumed low differential stress, extensional system). The vertical stress (S_v) was derived from estimated rock density and fluid pressures from an equilibrated pressure log. There were no mini-hydraulic fracture tests or rock strength measurements within the reservoir to use as inputs for the stress model. Instead, the analysis of the stress state was solved for iteratively by testing the sensitivity of breakout position and width to the azimuth of the horizontal principal stresses with respect to the unconfined compressive strength (UCS) of the formation, and then finding a range of stress magnitudes based on maximum horizontal stress (S_{Hmax}) azimuth and a range of UCS for representative basaltic rocks. This process was completed for each pair of breakouts identified within the image log and a variable stress regime is inferred as strike-slip near the surface, but changes into a transitional strike-slip-to-normal faulting regime at greater depths, with a mean S_{Hmax} azimuth of 026.6 ± 10°. This stress direction parallels the local graben-bounding faults, which strike 020 to 030, and the regional S_{Hmax} azimuth inferred from earthquake focal mechanisms, including strike slip focal mechanisms. However, we note that this borehole stress model is limited by relatively poor constraints on the magnitude of the minimum horizontal stress (S_{hmin}) and rock strength, which introduce significant uncertainty into the estimate of the S_{hmin} and S_{Hmax} magnitude distribution with depth. This state of stress suggests some of the natural fractures mapped in the well are optimally oriented for normal fault slip, but the injection area is likely within a strike-slip faulting regime.

INTRODUCTION

Despite Iceland's rich geothermal resources, active tectonics, and potential access to study the mechanics of the oceanic ridge rift and transform system, relatively few direct measurements of the stress state in Iceland are available (Figure 1). The image log from HN-16 in the Hellisheidi Geothermal Field, part of the Hengill Volcanic System (Figure 1) provides the opportunity to directly observe the stress state in an active rift system as well as the fractures that accommodate the deformation at ~1-2 km depth. In addition, despite active brittle deformation, geothermal systems are only intermittently localized along these rifts. Since it is expected that the stress and fractures combine to exert a strong influence on the permeability tensor and shape of the permeable volume (e.g., Heffer, 2002; Valley and Evans, 2007; Hickman and Davatzes, 2010; Davatzes and Hickman, 2009; Davatzes and Hickman, 2010b), we use this study as a first step in characterizing the stress associated with such active geothermal systems.

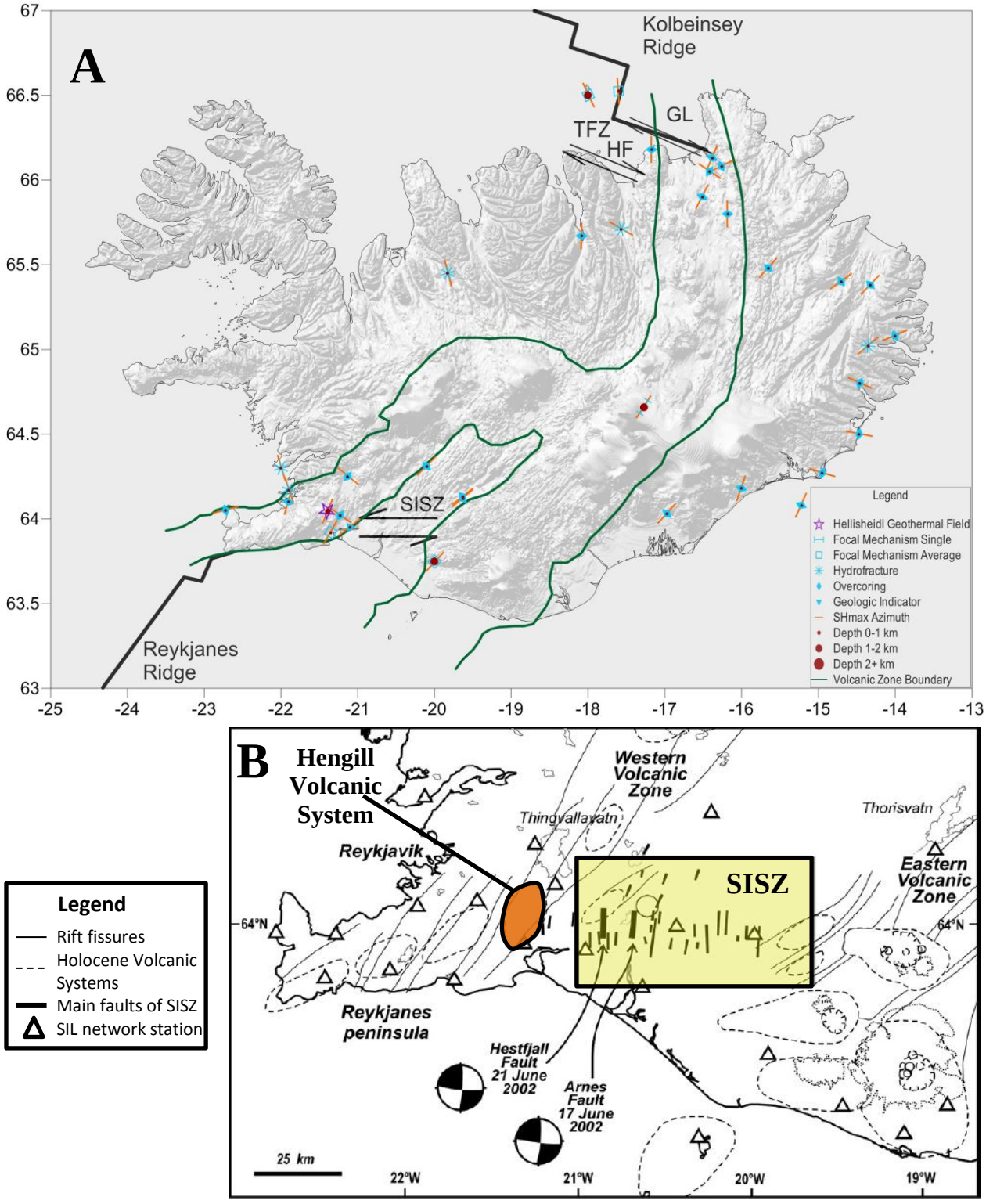

Figure 1. (A) Shaded relief map of Icelandic topography and major tectonic rift systems. The local azimuth of the most compressive horizontal stress, S_{Hmax}, is derived from borehole and geologic indicators of stress. Shown on the map are the Kolbeinsey Ridge, the Tjornes Fracture Zone (TFZ), the Grimsey Lineament (GL), the Husavik-Flatey Fault (HFF), the South Iceland Seismic Zone (SISZ), and the Reykjanes Ridge (Sykes, 1967; Haimson et al., 1977, 1982; Einarsson et al., 1977; Klein et al., 1977; Angelier et al., 2008; Heidbach et al., 2008; this study). (B) Map of Southwest Iceland with the SISZ and the Hengill Volcanic System highlighted. Two focal mechanisms just east of Hengill are shown (modified after Angelier et al., 2008)

From an operational perspective, the natural fracture population and stress also influence the expected direction of cold water breakthrough accompanying injection (Heffer et al., 1995; Willis-Richards et al., 1996; Heffer, 2002; Rahman et al., 2002) and the growth direction of stimulation (Schindler et al., 2008; Valley and Evans, 2007). In CO_2 sequestration projects, such as the nearby CarbFix Project (less than 3 km south and in the same structural zone as the Hellisheidi field), the stress field will determine the maximum pressure possible for injection without the danger of inducing a hydraulic fracture or significant slip within the natural fracture network, both of which have the potential for upward growth in normal and strike slip tectonic settings.

The Hellisheidi Geothermal Field in Iceland, part of the Hengill volcanic system, occupies an extensional rift characterized by young fissures at the surface. The reservoir is modeled as a fracture dominated volume extending along the graben-structure defined by these fissures (Franzson et al., 2010). Reinjection wells were drilled as part of a sustainability initiative, but had less than desired results. Well HN-16 had the highest injectivity rate with no clear answer why. This study used geophysical logs, including an image log in the highly deviated wellbore HN-16, to characterize the fracture population at depth and independently constrain the state of stress acting on the fractures intersecting the well and as a basis to characterize the stress state in the rift. We applied an iterative process to infer stress direction and magnitude from the occurrence, width and position of breakouts in the HN-16 borehole that takes into account the large borehole deviation from vertical and quantifies the uncertainty that results from the combined effects of the deviation, uncertainty in the rock strength model, and the lack of a mini-hydraulic fracturing test.

Results of this analysis help refine the reservoir model, inform future borehole design and any stimulation efforts to increase injectivity of other existing boreholes. Given the proximity of the CarbFix carbon sequestration project, the constraints on the fracture network and stress state from this study are also relevant to management of injection pressures in that sequestration reservoir.

GEOLOGIC SETTING

Iceland

Iceland is a unique island, sitting atop the Mid-Atlantic Rift and a mantle plume. This setting gives Iceland its extensive geothermal resources throughout the country. A simple tectonic model for the country is the extensional rift splitting the island; however, it is more complicated than a simple rift model (Sykes, 1967; Einarsson et al., 1977; Haimson and Voight, 1977; Klein et al., 1977). As seen in Figure 1, the main rift zone is split into two sections in the south of Iceland, one along the Reykjanes Peninsula and one further east that includes the recently erupted Eyjafjallajokull. These branches merge in the middle of the country and continue as a single zone to the north offshore in the Tjornes Fracture zone. The two southern rift zones are connected by the South Iceland Seismic Zone (SISZ). The pattern of geologic faulting and focal mechanisms studies indicate that the SISZ is a left-lateral Riedel shear structure (Hardarson et al., 2010; Khodayar and Bjornsson, 2010). Relatively few studies directly measure the stress field despite this complex tectonic structure. Hast (1969) conducted overcoring experiments in several localities, all less than 100 m deep, and Haimson and Voight (1977) and Haimson and Rummel (1982) produced hydrofracturing results, but only to depths less than 600 m. In the region's studies, topography is likely to strongly influence these stress measurements at the shallower depths. There have also been some focal mechanism inversion studies throughout Iceland, but these largely represent "averages" of the primary seismic zones, which is geographically extensive, thus providing little information on the detailed tectonic picture or on the scale of a single geothermal system. All previous stress studies are displayed on Figure 1 with labels indicating the type of stress measurement (Hast, 1969; Haimson and Rummel, 1982; Haimson 1979; Haimson and Voight, 1977;Dziewonski et al., 1997; Miller et al., 1998; Khodayar and Bjornsson, 2010; Angelier et al., 2004; Angelier et al., 2008; Lund and Townend, 2007; Lund and Slunga, 1999). The focal mechanism data is perhaps most reliable for Iceland, although averages, because it is the deepest data and could represent broad tectonic trends. The remaining studies derived from surface expressions of faults and fractures or shallow boreholes are arguably too shallow to infer crustal stress patterns.

Hengill Volcanic System

The Hellisheidi geothermal power plant is located in the southern part of the Hengill volcanic system, on the western flank of the South Iceland Seismic Zone (SISZ) (see Figure 2). The Hengill region is the largest active volcanic system in Iceland at nearly 110 km^2, and is located at the triple junction of two active rift zones and a transform fault. The majority of the Hengill volcanic system is comprised of hyaloclastite formations representing the central volcano underlain with lava flows interpreted as the base of the Hengill volcano. There have been three Holocene eruptions; the two most recent eruptions (five and two thousand years ago) are associated with the geothermal fields and are centered in the graben (Franzson et al., 2010; Saemundsson, 1995a; Saemundsson, 1995b). Fissure swarms associated with the eruptions are thought to be the major fluid flow paths for production wells within the Nesavellir Geothermal Field (northeast of the study area) and the Hellisheidi Geothermal Field (Franzson et al., 2010; Hardarson et al., 2010). MT and TEM soundings have revealed deeper anomalies running in a WNW-ESE direction (Arnason et al., 2000; Arnason et al., 2009). These anomalies are low resistivity bodies that occur at 4 km depth and greater, deeper than any wells in the Hellisheidi geothermal system. The meaning of the anomalies is unclear, but has been hypothesized as a zone of partial melting or supercritical fluid and may have a role in supplying hot fluid to the reservoir (Arnason et al., 2009). The dominant structure, however, is the NE-SW running graben structure that contains the recent fissure swarms (Franzson et al., 2010; Arnason et al., 2009). The graben is associated with a high density of en-echelon fault segments of the same NE-SW strike that are the primary target for both reinjection and production wells as they are significant fluid flow paths similar to the fissure swarms from recent volcanism(Bjornsson, 2007; Franzson et al., 2010).

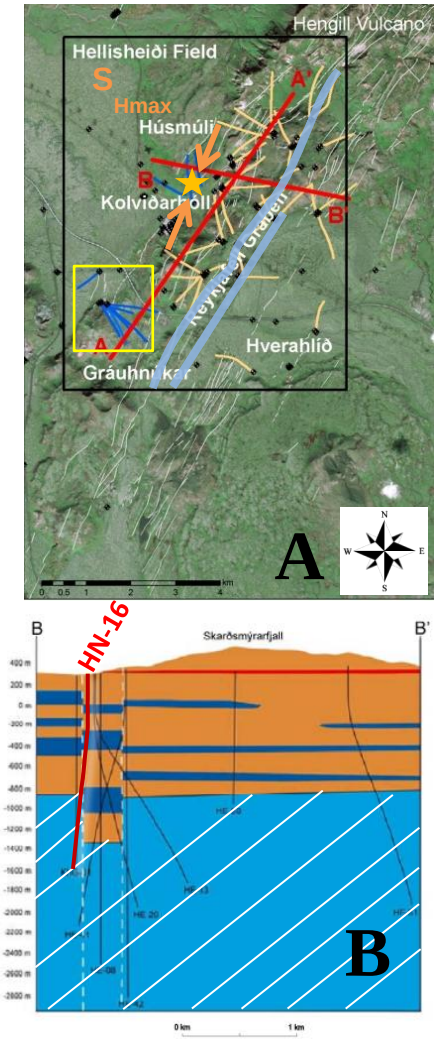

Figure 2. (A) The Hellisheidi Geothermal Field in the Hengill Volcanic System. The location of well HN-16 in the Kolvidarholl-Husmuli reinjection area is, approximately located by the star. Production well paths are represented by yellow lines, whereas blue lines are the paths of reinjection well. The yellow box outlines the approximate location of the CarbFix project. The thin white lines map fault scarps associated with the Hengill graben. The thick red lines are cross section presented in Hardarson et al. (2010). The orange arrows show the direction of S_{Hmax}, and the light blue lines are the location of the Holocene lava eruptions associated with the geothermal field. Hverahlid can be seen in the bottom right of the black box outlining the Hellisheidi Geothermal Field (Modified after Hardarson et al., 2010). (B) Cross section B-B' showing the structural model of the geothermal field (Modified from Hardarson et al., 2010).

Studies of the thermal evolution summarized by Franzson et al. (2010) state that Hengill is believed to have reached peak thermal output during the last glacial period of Iceland around ten to fifteen thousand years ago based on temperature logs and subsurface alteration horizons. While the entire volcanic system is now in a cooling stage, there were local heating episodes along the Holocene fissures centered within the graben associated with lava eruptions five and two thousand years ago. The eastern side of the volcanic zone is cooling at a higher rate interpreted to result from increased permeability and fluid circulation in the South Iceland Seismic Zone. Hverahlid to the south has a separate high temperature anomaly which is not associated with the Holocene fissure swarms and lava eruptions, requiring an additional localized heat source in addition to the cooling Hengill volcanic system in that location (Franzson et al., 2010, Nielsson and Franzson, 2010).

The tectonic model of the Hengill volcanic zone is primarily interpreted from surface fault scarps. There has been one focal mechanism study within the study area using an array of 23 vertical 1 Hz seismometers locally deployed, which suggests approximately 75 percent of seismic activity is related to tensile cracking caused by cooling and the other 25 is from pure shear ; the stress directions (035 S_{Hmax} azimuth) were consistent across the array area and support an extensional rifting environment model (Foulger, 1988). The stress state inferred from the focal mechanism study is also comparable with recent earthquake fault scarps from a May 2008 earthquake (060-045 modeled S_{Hmax} azimuth) that has a trend consistent with the Riedel shearing model for the SISZ (Miller et al., 1998; Khodayar and Bjornsson, 2010). These data form the tectonic model for the area, and when combined with drilling data, can inform future drilling projects.

Hellisheidi Geothermal Power Plant

The Hellisheidi geothermal power plant is a combined heat and electrical power generating facility with a single flash power cycle. The installed capacity of the plant is 303 MWe, 130 MWt. The thermal output can be increased to 400 MWt to provide heating for future industries. At present there are 57 production wells at depths of 1,300-3,300 m and 17 reinjection wells with other exploration or cold water wells that are not mentioned (Hardarson et al., 2010). One goal of the power plant is reinjection of all effluent water production, which is near 586 l/s at full capacity. The seventeen reinjection wells have been drilled in two separate fields: Husmuli in the northern part of the geothermal field, and Grauhnukar to the south, as seen in Figure 2. At the time of this study, well HN-16 was accepting the most fluids of any reinjection well near 200 l/s, but total reinjection from all injection wells was still below the desired 500 to 600 l/s. In October 2010 well HN-17 was drilled and surpassed the desired injection capabilities. Several tests were conducted by Reykjavik Energy with the original goal of increasing the injectivity of under-performing wells including varying injection temperature and rate of injection (Hardarson et al., 2010; Franzson et al., 2010). Included among the tests to improve injectivity and plan future wells, the Borehole Televiewer (BHTV) data referenced in this study was collected from HN-16 in October 2010. HN-16, like most of the injection wells in the field, is a deviated well. HN-16 is deviated up to 37° from vertical directed north and is drilled to a measured depth of 2,204 m. In addition to the BHTV log, the well is characterized by an un-calibrated borehole compensated neutron porosity log, a natural gamma ray log, a gyroscopic deviation log, temperature and pressure logs, as well as the mud log which includes a detailed lithologic and alteration log. Although this analysis focuses on HN-16, other wells in the vicinity of HN-16 provide the opportunity for future data collection.

NATURAL FRACTURES

The image log was acquired October 17th, 2010 using the ALT ABI-43 acoustic imaging tool during an inject-to-cool operation to accommodate the upper operating limit (125-135°C) of the tool. Given the high concentration of magnetic minerals in at least some basaltic layers penetrated by the borehole, the deviation data typically acquired through the magnetometer integrated in the BHTV was corrected against an independent gyroscopic log. This allowed unambiguous conversion of the apparent strike and dip of structures into true strike and dip. Interpretation of the fractures and processing were carried out in the software WellCAD produced by the company ALT.

Natural fractures (NF) are identified in the "unwrapped" BHTV image log as a sinusoidal trace of reduced acoustic amplitude or signal loss due to scattering of the acoustic pulse caused by the roughness at the intersection with the borehole (Figure 3a). Throughout the well there is a small variation in the azimuth and true dip direction of the fractures (Figure 4), but as a whole the fractures intersecting the borehole strike NNE-SSW dipping nearly vertical to the east. These findings are similar to results of previous fracture studies in the area (Blischke, pers. comm., 2010-11; Hardarson et al., 2010; Foulger, 1988) and mimic the trend of the graben.

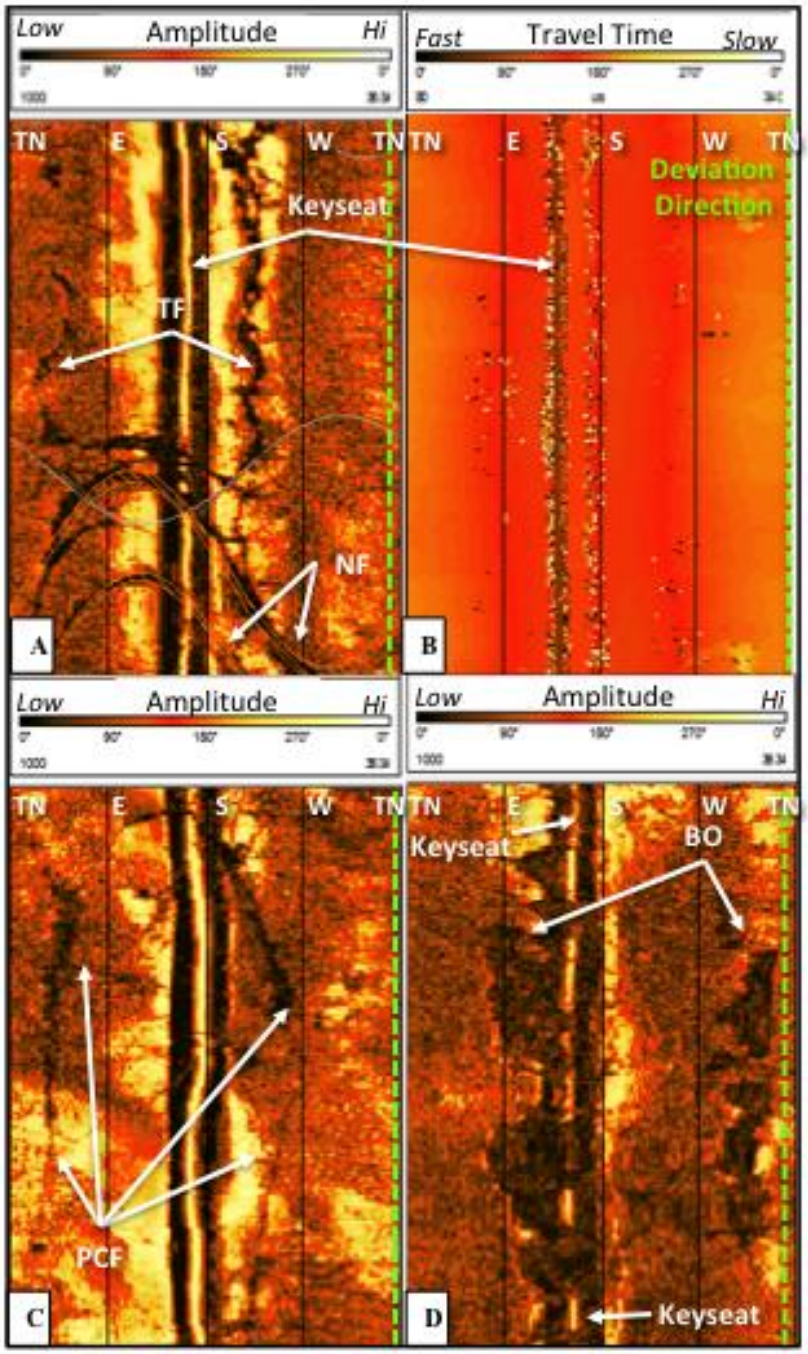

Figure 3. Examples of (A) sinusoidal trace of natural fractures(NF) intersecting the borehole wall, and tensile fractures, (TF)at 1910m measured depth (MD); (B) possible borehole cross-sectional elongation in the travel time image at 1700m MD; (C) petal-centerline fractures (PCF) at 2122m MD; and (D) breakouts, (BO) at 1687m MD. All MD shown here are from the Kelly bushing and not ground level. (A-D) Note the significant pipe wear known as a "keyseat" in each image common to highly deviated boreholes. Both TF and BO wall failure form 180^o, however, BOs have discrete azimuthal width. Lower amplitude often indicates signal loss due to acoustic scattering at a rough borehole wall due to an open fracture or broken rock in that spot or non-normal incidence of the acoustic pulse at the edge of features such as keyseats. In an inclined borehole, breakouts do not strictly correspond to the azimuth of S_{hmin}, nor do tensile fractures correspond to the direction of S_{Hmax} as they do in a vertical well.

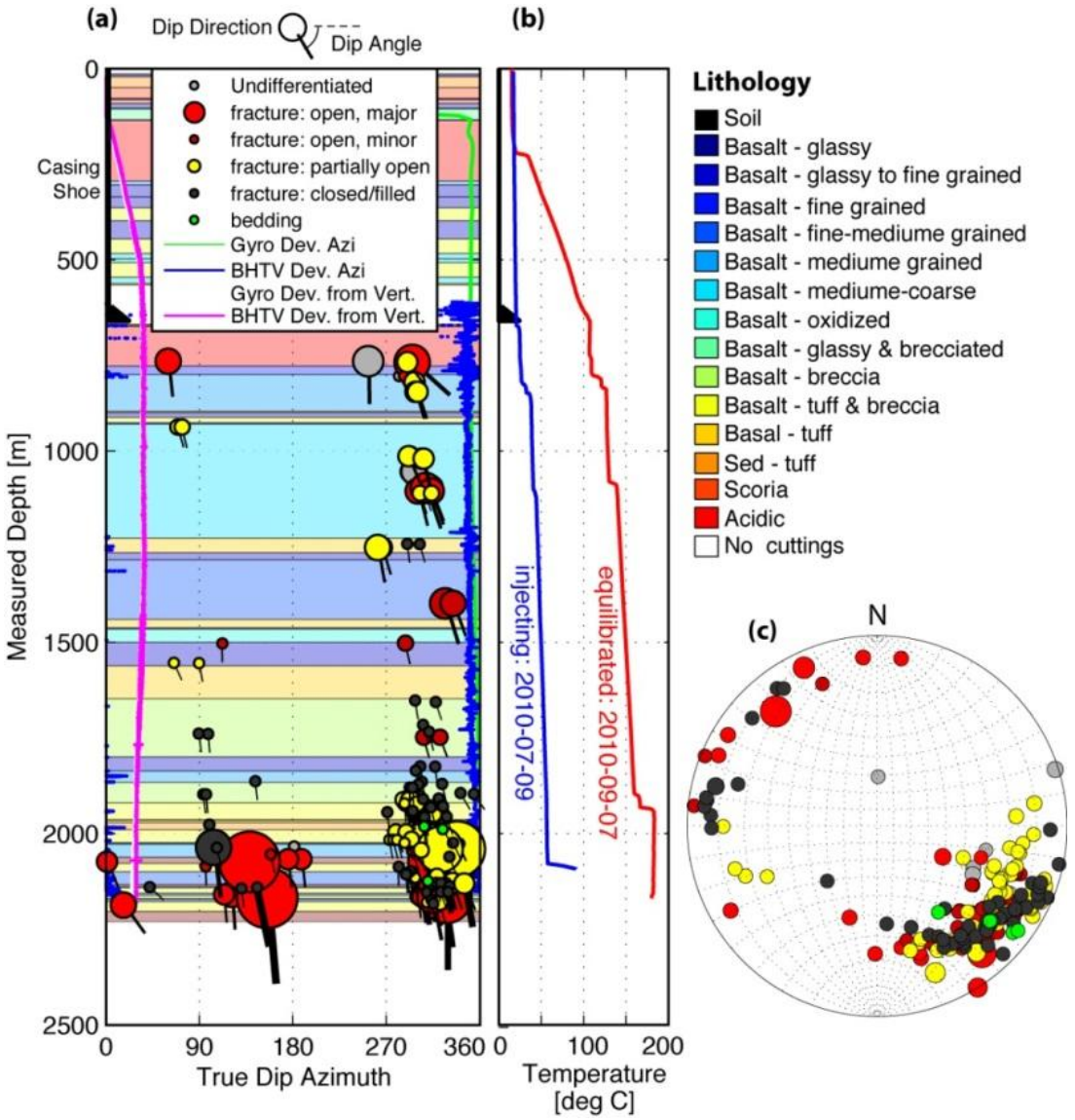

Figure 4. (a) Tadpole plot of Natural Fracture network showing dip direction and angle overlaid on the cuttings log with well deviation data. Tadpole size is related to apparent aperture as interpreted on the BHTV log (b) Temperature logs during injection and an equilibrated log showing major flow zones. (c) Southern Hemisphere polar plot of the natural fractures showing there are two distinct fracture populations that are both steeply dipping.

STRESS FIELD MODELING

Drilling Induced Deformation

The image log in HN-16 reveals extensive drilling induced deformation evident as borehole wall breakouts and tensile fractures (e.g., summarized in Zoback et al., 2003) and petal-centerline fractures which form below the borehole floor during drilling (Davatzes and Hickman, 2010a; Garza-Cruz and Davatzes, 2010). These structures result from the concentration of stress at the free surface of the borehole and can be used to model the stress state in the volume penetrated by the borehole. Breakouts are the most abundant drilling induced structure in the HN-16 borehole, and are used to develop the stress model (Figure 3). There were tensile cracks, but in sparse quantity and current models for tensile formation within geothermal wells with extensive cooling, as in this well, perform poorly given our current understanding. Similarly, there were a high number of petal-centerline fractures, but modeling their formation within a deviated borehole is still in development. Breakouts were identified by: 1) occurring in pairs 180° apart, 2) having a dog-eared cross-sectional geometry, and 3) having irregular margins reflecting grain or layer-scale variation in rock strength, as described in detail by Zoback et al.

(2003) and Davatzes and Hickman (2010a) (Figure 3). Because the borehole is inclined we cannot assume one principal stress is aligned with the borehole axis as is typically done in vertical wells in which the weight of overburden is taken as a principal stress consistent with Andersonian mechanics (Peska and Zoback, 1995). In this case the occurrence of breakouts is a function of all three principal stress directions and magnitudes as they are resolved onto the borehole surface through a matrix transformation, as well as the borehole conditions including the mud pressure, formation fluid pressure, thermal stresses, and the rock strength that resists failure. The combination of these contributing factors controls the occurrence of breakouts as well as their position relative to the high side of the borehole and their width, which corresponds to the region over which the compressive strength of the rock has been exceeded due to the concentration of normal compressive stress tangential to the borehole wall (hoop stress). The position and width of breakouts relative to the top-side of the borehole is derived from the oriented image log.

Modeling Breakout Formation

The magnitude of the vertical stress (S_v) is derived by integrating the overlying bulk density of rocks as guided by the lithology log in Gudfinnsson et al. (2010) and representative mean densities for these rock types compiled from the literature (Figure 5) and correction of the measured depth (MD) to the true vertical depth (TVD). The fluid pressure distribution in the formation (P_p) is derived from an equilibrated fluid pressure log measured on September 7th, 2010. Figure 6 gives derivations of the boundaries to the model and a statistical analysis of the breakouts. In modeling the stress state from the occurrence of breakouts, we model the borehole conditions most favorable for breakout formation between the time of drilling and acquisition of the image log. Breakout formation is promoted by mud pressures (P_m) that "under-balance" formation fluid pressure thereby enhancing compression tangential to the borehole wall, and heating (through hot water production) that causes thermal expansion and similarly increases compression. In HN-16, the most favorable conditions prior to logging correspond to $P_m = P_p$ and no cooling, both of which were achieved by the time of the equilibrated pressure log. To our knowledge, no intense production or air-lift operations occurred that would produce lower P_m magnitudes or heating of the borehole.

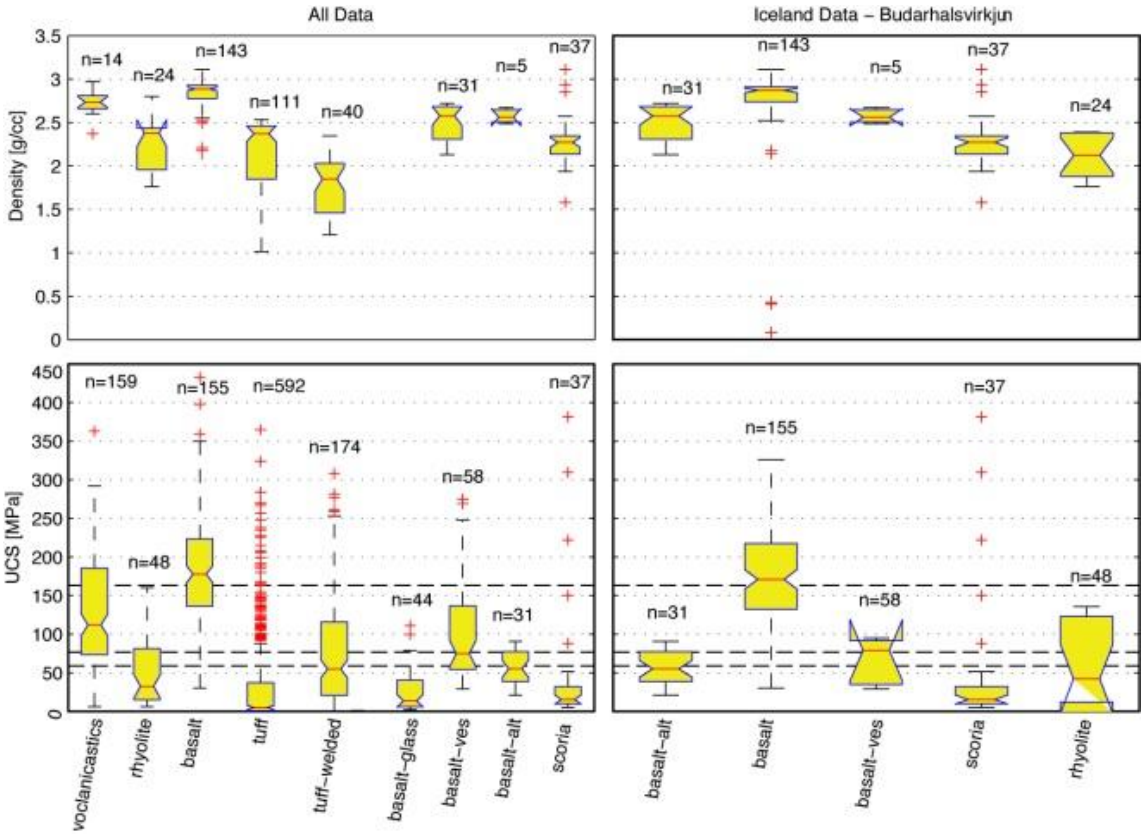

Figure 5. Box plots of density and unconfined compressive strength (UCS) for basaltic rocks (Moos and Pezard, 1996; Arngrimsson and Gunnarsson, 2009; and Davatzes and Hickman, 2011). The density model for vertical stress (S_v) and the three UCS used for modeling come from this data compilation. The abbreviations "ves" and "alt" are vesicular and altered, respectively.

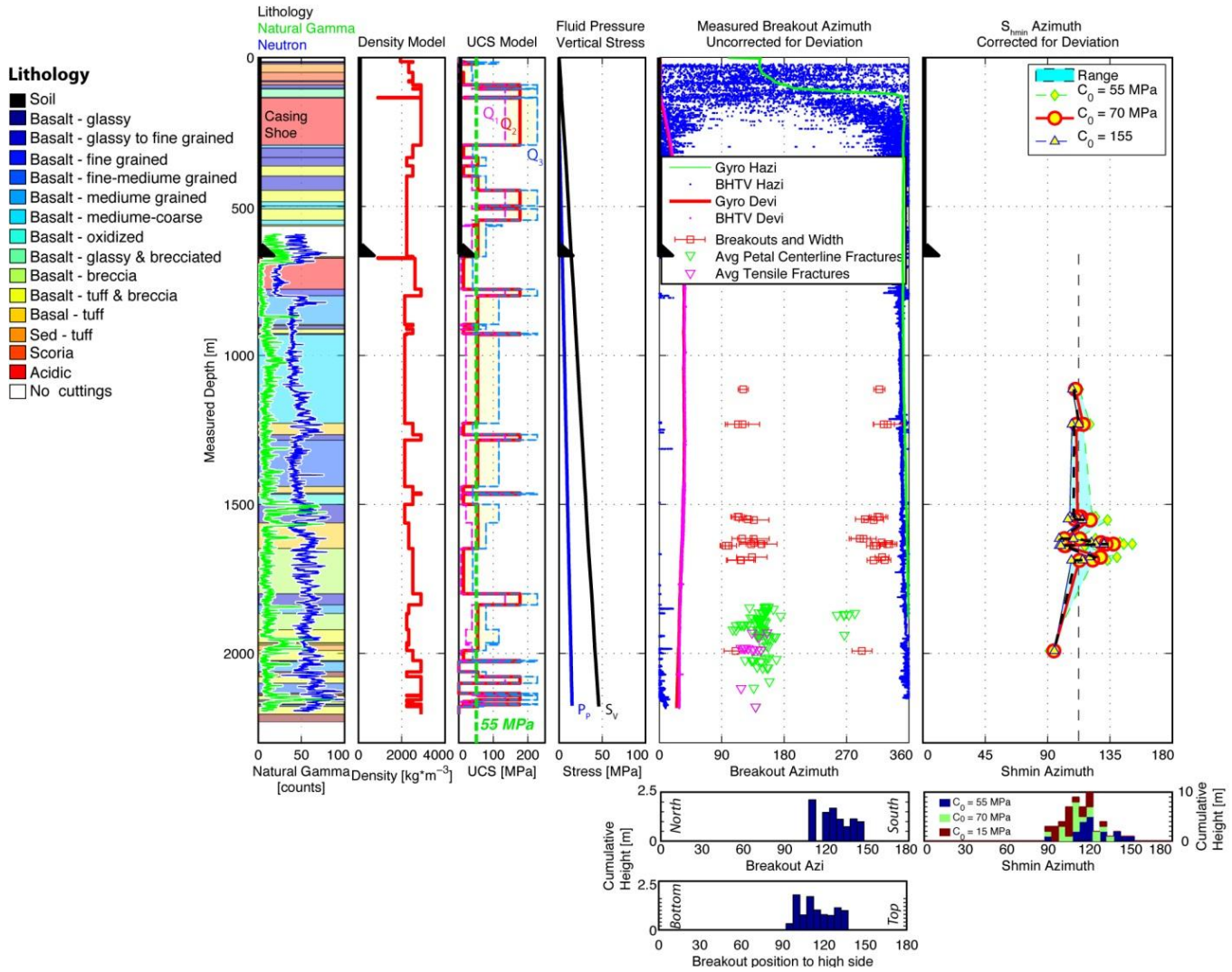

Figure 6. Top, from left to right: Lithologic log with Natural Gamma Ray API counts and uncorrected Neutron porosity log overlain; density model derived from literature and lithologic log; UCS model derived from literature and lithologic log; S_v model derived from density model and fluid pressure log; drilling induced structures found within the borehole showing azimuth and width; modeled range of S_{hmin} azimuth for UCS = 55, 70, and 155 MPa. Below, statistical data testing for heterogeneity of the breakout sample set. Breakout azimuth is uniform implying small changes in the stress state while there is no correlation between UCS and resulting S_{hmin} azimuth showing stress direction is insensitive to UCS between 55 and 155 MPa.

Modeling of the S_{Hmax} Azimuth

The modeling of the two principal horizontal stress magnitudes and the azimuth necessary to produce the breakouts of the observed width and position in the highly inclined HN-16 well was conducted using the software Stress and Failure of Inclined Boreholes (GMI·SFIB) designed by GeoMechanics International (GMI). This software solves the stress boundary value problem deriving: (1) the remote stress tensor onto the borehole surface and (2) the local sources of stress due to the (a) mud pressure in the borehole, (b) thermal stress accompanying temperature change through the coefficient of linear expansion, and (c) the poroelastic distortion adjacent to the borehole wall through Biot's coefficient and Poisson's ratio. The software then compares the stress distribution along the borehole surface to the constraints on breakout initiation for the unconfined compressive strength and the Mohr-Coulomb parameters of the internal friction and cohesion, used to evaluate breakout propagation.

However, this problem cannot be solved uniquely in the absence of an independent constraint on one of the principal horizontal stress magnitudes, the azimuth in which these stresses act, and the rock strength. Alternatively, multiple borehole orientations containing breakouts in close proximity can be used as additional constraints if the stress state is assumed homogeneous within the combined sample volume. In this initial study, we lack both an in-situ strength model constrained by rock mechanical testing of the rocks penetrated by the borehole and indexed to in-situ geophysical logs such as sonic velocity or porosity to account for natural heterogeneity (e.g., see discussions in Zoback et al., 2003 and Davatzes and Hickman, 2011) and a direct measurement of a horizontal stress magnitude as might be provided by a mini-hydraulic fracture.

To address the missing rock strength model, we compiled a data set of rock properties from the literature and consistent with the lithologic log from HN-16 (Figure 5). This analysis indicated we should consider three distinct magnitudes of unconfined compressive strength representing the median values for the predominant rock types: unaltered basalt, 155 MPa; intermediate or vesicular basalt, 70 MPa; altered basalt, 55 MPa (Moos and Pezard, 1996; Arngrimsson and Gunnarsson 2009; Davatzes and Hickman, 2011 and references within). In the extremity, these populations span UCS from 1 to 275 MPa, and some rock types like scoria are more generally weak, and others such as "basaltic breccia" are uncertain. To address the lack of a definitive S_{hmin} magnitude, we adopt an iterative approach in which we: (1) first solve for permissible horizontal principal stress directions at a range of S_{hmin} magnitudes and rock strength (UCS); (2) Second we solve for the magnitudes of the horizontal principal stresses. In both cases, we map the uncertainty that results from the UCS model and the S_{hmin} magnitude.

In this first step we evaluated S_{hmin} magnitudes ranging from critically stressed for normal faulting at a coefficient of friction of 0.8 to one in which S_{hmin} approaches S_V, thus spanning the range of stresses consistent with normal faulting to strike-slip faulting. The 0.8 coefficient of friction is a conservative estimate based on frictional strength studies of the crust, whereas oceanic basalts are expected to have a coefficient of friction of 0.65 (Table 1). For this range of S_{hmin} magnitudes we derived corresponding S_{Hmax} azimuths consistent with breakout position and width for each pair of breakouts in the borehole as a function of rock strengths (UCS) (Figure 7). The physical properties and borehole conditions used in these plots are summarized in Table 1. We find the majority of breakouts are consistent with an S_{Hmax} azimuth of 022.4±5° (or an equivalent S_{hmin} azimuth of 112.4±5°) if UCS exceeds 55 MPa (Figure 6) consistent with the expected range of UCS inferred from the rock types (Figure 5). In other words, the sensitivity of the S_{Hmax} azimuth to S_{hmin} magnitude was small for a UCS between 55 and 155 MPa; below 55 MPa, the stress direction varied between 010 and 060. In general, higher UCS produces less variability in the inferred S_{Hmax} azimuth. This is reflected in the formal error in S_{Hmax} azimuth derived from propagating the precision of correlation between UCS and S_{Hmax} azimuth with the standard deviation of the sub-population of local S_{Hmax} azimuths derived from breakout pairs at each UCS value shown in Table 2). Other strength parameters including the internal friction were varied in the range from 0.4 to 1.1 without changing this result.

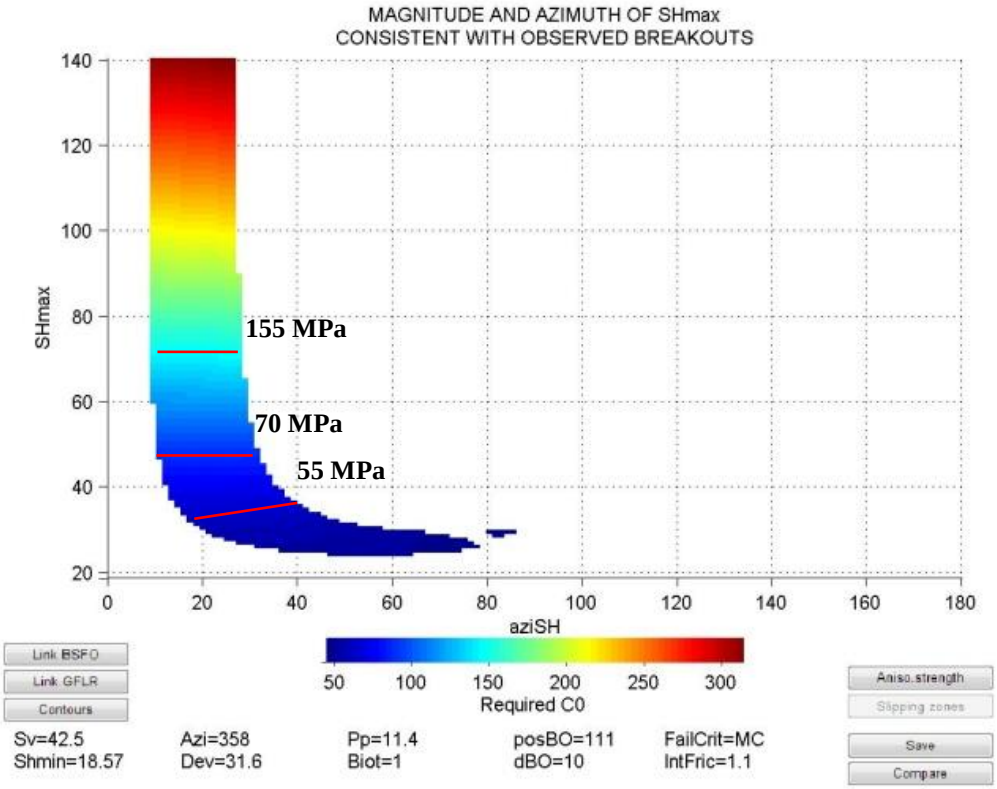

Figure 7. Output image from first GMI·SFIB module. Different values of UCS representative of un-altered basalt, 155 MPa, glassy basalt, 70 MPa, and altered basalt, 55 MPa, are shown by the red lines. S_{Hmax} azimuth is uniform and insensitive to UCS until values approaching 55 MPa and lower. These output values of S_{Hmax} azimuth were then used to calculate the possible stress magnitudes using a second GMI·SFIB module.

Table 1. Input Physical Properties and Borehole Conditions.

Property	Magnitude	Notes	Source
Internal Friction, μ_i	0.8	Sensitivity tested 0.4 to 1.1	Schön (1996), Jaeger and Cook (1979)
Cohesion	30 MPa		Schön (1996) , Jaeger and Cook (1979)
Unconfined Compressive Strength, UCS	55, 70, 155 MPa	Evaluated for three most prevalent rock types	Compilation of literature: Oceanic Basalt and Icelandic Basalt
Poisson's Ratio, υ	0.25		Assumed (insensitive)
Biot Coefficient	1		Assumed (insensitive)
dT	0°C, to -100°C	The most positive dT promotes breakout	Drilling History
Linear coefficient of thermal expansion, α	6×10^{-5}	Oceanic Basalt	Schön (1996)
Borehole Mud Pressure, P_m	$P_m = P_p$	Mud Weight; balanced	Drilling history
Formation Fluid Pressure, P_p	Pp	See Figure 6	Equilibrated Pressure Log
Vertical Stress, S_V	S_V	See Figure 6	Integrated weight of overburden; lithologic model is from the mud log; densities are from the literature
Coefficient of Friction, μ_s	0.65 0.8	Oceanic Basalt Byerlee Friction	Boettcher et al., 2004; 2007; Brace and Kohlstedt (1980), Byerlee (1978), Hearst (2000)

Table 2: Results of analysis of S_{Hmax} direction for assumed UCS

Generalized Rock Type	Assumed UCS	Circular Mean S_{Hmax} Azimuth	Estimated Precision	Standard Deviation	Propagated Error
Altered Basalt	55 MPa	034.7	~21°	14.3°	25.4°
Intermediate Basalt	70 MPa	024.9	~7°	11.5°	13.4°
Un-Altered Basalt	155 MPa	020.1	~5°	9.8°	10.6°

The logged variation in rock types, as well as in the neutron count and natural gamma count indicate variability in the UCS of formations in which breakouts occur. In particular, the neutron count is sensitive to porosity, which is known to influence UCS (e.g., Price et al., 1993; Li and Aubertin, 2003; see also discussions in Zoback et al., 2003 and Davatzes and Hickman, 2011). However, consistency in the position breakouts at a variety of depths suggests this variation must occur for UCS in excess of 55 MPa, for which the S_{Hmax} azimuth is stable. Thus, it is reasonable to assume the derived S_{Hmax} azimuth is a robust result. Alternatively if all breakouts occur in rock with UCS less than 55 MPa despite these lithologic differences, then the S_{Hmax} azimuth could range from 010 to 060 (Figure 6), leading to a nearly complete lack of constraint on the S_{Hmax} azimuth. Although we expect breakouts to preferentially form in relatively weak rock, we consider this latter alternative unlikely since similarities in breakout position within an inclined well are very sensitive to small variations in UCS. Thus the UCS would have to be very similar in all cases, inconsistent with the variability in the rock types and geophysical properties.

Modeling of the Principal Horizontal Stress Magnitudes

Second, using the derived S_{Hmax} azimuth, we determined the combinations of S_{hmin} and S_{Hmax} magnitudes that together with S_V, P_p and the borehole conditions could reproduce the breakout positions and widths (Figure 8). These results were also checked against the inputs to the calculation of S_{Hmax} azimuth to ensure internal consistency. The polygon in Figure 8 defines the range of principal horizontal stress magnitudes scaled to the vertical stress that can be supported by the frictional strength of the crust, conservatively estimated to be 0.8. The UCS necessary to allow the modeled breakout to form is contoured as a function of these principal horizontal stresses; only the ranges of S_{hmin} and S_{Hmax} capable of producing breakouts are contoured. Where the contours intersect the outer margin of the polygon indicate stress states that are "critically stressed" for slip on optimally oriented fractures, whereas interior positions represent "stable" or "under-stressed" states.

For each breakout, the "critically stressed" and the "stable" values were collected for the three representative UCS magnitudes of 55, 70, and 155 MPa. For any given breakout, the span along a UCS contour represents the range of horizontal stress magnitudes scaled to S_V that are consistent with the breakout occurrence and thus is a measure of the uncertainty in the stress magnitude model. The resulting stress model as a function of depth is plotted in Figure 9 for the three representative UCS magnitudes. Using a similar approach, combining contours define polygons that outline the permissible ranges of stress magnitudes within the stress polygon (Figure 8).

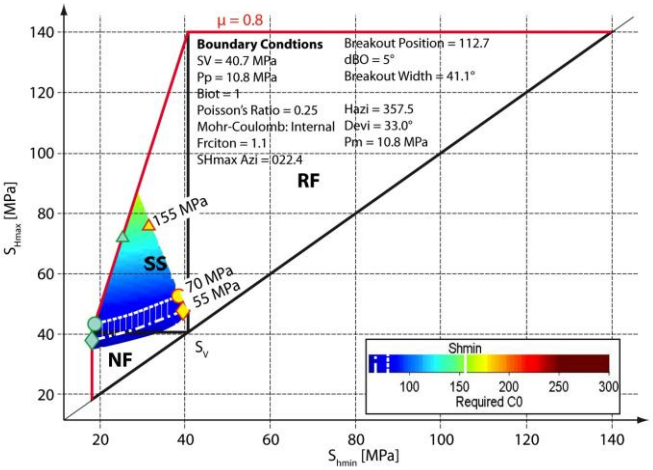

*Figure 8. Output image from module 2 of GMI*SFIB. The red line is the frictional failure envelope and anything outside of the stress polygon is unstable and would be actively faulting. The green shapes represent the "critically stressed" stress state while the yellow shapes represent the "stable" stress state. These values were picked for three different UCS, but the most likely stress states lie within the shaded region based on cuttings and alteration data for well HN-16.*

Summary of Stress Modeling

A total of eighteen breakouts were identified on the BHTV image log and a respective stress state was modeled capable of inducing each within the borehole wall. The S_{Hmax} azimuth was quite uniform for a UCS of 70-155 MPa. For a UCS of 55 MPa there was more variation, but all azimuth values for a given breakout are within ±21°. The larger range in azimuth for 55 MPa invalidated the original plan of modeling the stress magnitudes with an average azimuth; instead, for the UCS of 55 MPa, each breakout was modeled using a locally calculated azimuth rather than an average azimuth.

Figure 9 summarizes the potential 3D stress models for this well. The assumption of a relatively low UCS of 55 MPa (Figure 9a) produces a stress regime transition from normal to strike slip, as does a UCS of 70 MPa (Figure 9b), although with slightly greater potential for differential stress as well as uncertainty in the ranges of permissible of S_{hmin} and S_{Hmax} magnitudes. In both cases, the shallower cluster of breakouts is consistent with a more strike slip stress state than deeper breakouts, which tend toward normal faulting. A UCS of 155 MPa (Figure 9c) essentially requires strike slip faulting stresses. In all three cases, the greatest uncertainty is associated with S_{hmin} due to the large difference between the critically stressed and stable magnitudes that can still produce breakout (Figure 8).

The range of 55 to 155 MPa is a reasonable range for UCS based on the published values for basaltic rocks (Figure 5), especially for Icelandic basalt. The highlighted box indicates the possible stress states for a given UCS of 55-70 MPa, which is believed to be most representative of the rock types in which breakouts occur given a review of the literature. There is potential for locally lower UCS associated with scoria, or perhaps brecciated basalts, but these do not apply to the population of breakouts as a whole. In addition, the more detailed strength model derived from rock type in Figure 6 suggests that at least some breakouts must occur in high UCS materials, providing a strong constraint on S_{Hmax} azimuth, as well as a need for a higher differential stress, strike slip stress state. Nevertheless, a wide range of stress states could cause these breakouts, and most of these stress states are transitional between normal and strike slip faulting. Normal faulting can occur but only seems likely in the regions of the crust critically stressed; however, strike slip faulting will be more prevalent.

The most notable outcome observed is a change in the faulting regime with depth. If the crust is assumed to be critically stressed, consistent with young fault scarps and local earthquake activity, then the breakouts show a general trend from the transitional normal-to-strike slip faulting regime at shallow depth to a normal faulting regime at greater depth (Figure 9d). In either case, the direction of S_{hmin}, is most consistent with normal faulting on the natural fracture population (Figure 4), despite the steep dips of the fractures. Currently, the uncertainty in the stress magnitude model prevents further exploration of this relationship.

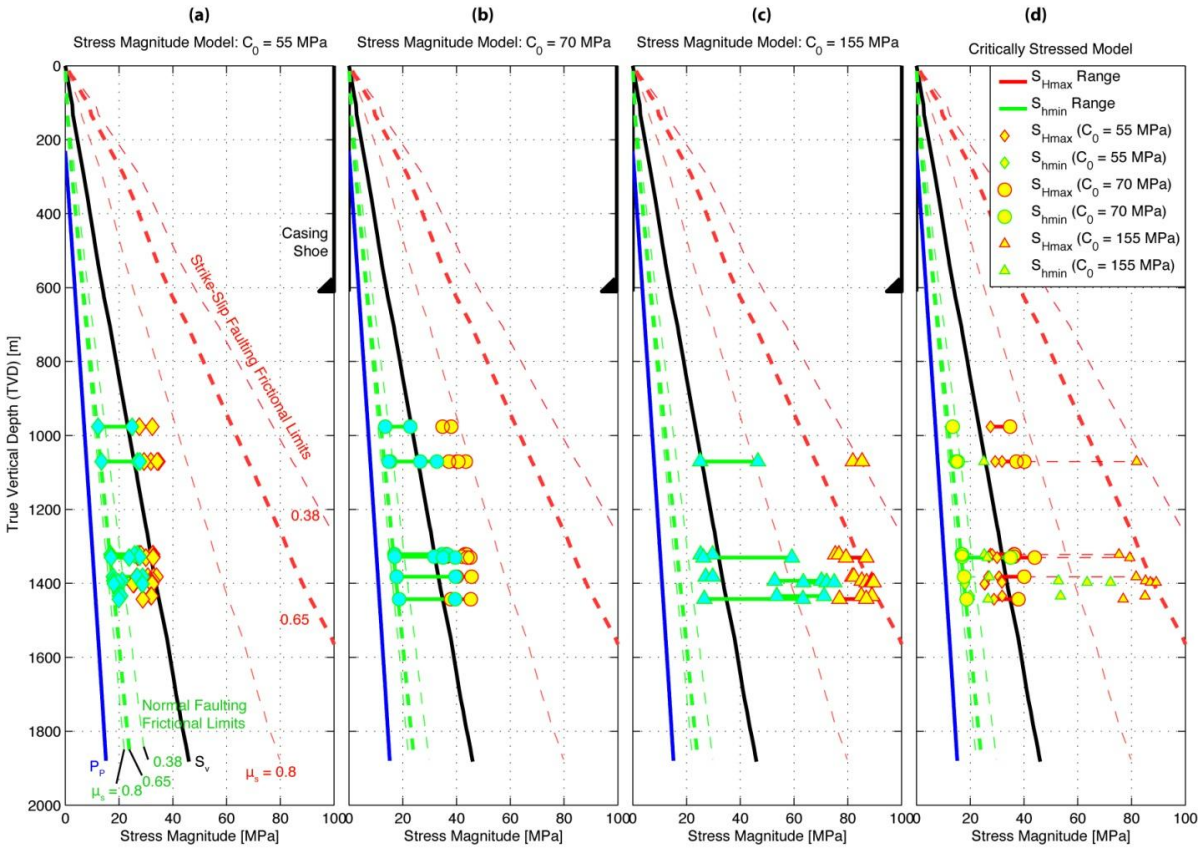

Figure 9. (a) Stress model for a UCS = 55 MPa, (b) Stress model for a UCS = 70 MPa, (c) Stress model for a UCS = 155 MPa, and (d) Stress model for a critically stressed crust. Green lines represent the normal faulting frictional limits for a given coefficient of friction, and the red lines, the strike-slip faulting frictional limits. As UCS increases, the possible range of stress magnitudes increases, emphasizing the need for an independent constraint on stress magnitudes either in the form of a UCS measurement or a mini-hydrofracture. The critically stressed model implies a change in the faulting regime with depth from transitional strike slip-to-normal faulting to a normal faulting regime for a crust at the failure envelope.

DISCUSSION

The stress model developed for this study using BHTV and other available data shows there is a large range of horizontal principal stress magnitudes that can account for the occurrence of breakouts at the depths and widths seen within this well. However, the horizontal principal stress direction appears to be well-defined and stable within the plausible range of UCS.

A primary assumption driving interpretation of the stress model is that the crust is critically stressed in this region leading to the inference of a changing stress regime at depth in Figure 9. A critically stressed crust for the area surrounding the Hengill Volcanic System is supported by the presence of Holocene fault scarps and existing seismicity with focal mechanisms and attitudes consistent with the modeled stress state in this study (Miller et al., 1998; Khodayar and Bjornsson, 2010). The critically stressed assumption helps refine the model, indicating the lower bound is closer to reality.

Recommendations

The fracture and stress model developed for this study provides a solid foundation for understanding the conditions impacting injectivity in HN-16, but there are opportunities to greatly improve this assessment:

(1) A refined UCS model would decrease the range of permissible stress magnitudes to produce the imaged breakouts and increase confidence of the range in S_{Hmax} azimuth. This could be accomplished using a porosity log or velocity log and correlating it to UCS measurements. In this regard, the uncalibrated Neutron porosity log provides a practical opportunity and should be processed providing, in combination with the detailed lithology log, a sound basis for such a model. We note here though, that velocity logs show the strongest

correlation to UCS (Hearst et al., 2000). This has been discussed in the literature and comparisons for rocks within Iceland do exist (Frolova et al., 2005; Arngrimsson and Gunnarsson, 2009). Such a model would greatly benefit from a direct measurement of the rock strength using representative rock samples from the formations containing the breakouts.

(2) A direct measurement of the S_{hmin} magnitude through a mini-hydraulic fracture test would greatly improve the accuracy of the stress model. This constraint would improve the calculation of the azimuth of the horizontal principal stresses over the estimated range of S_{hmin} magnitudes tested and improve resolution of the S_{Hmax} magnitude.

(3) The final possibility is image data containing breakouts within a nearby well with a distinctly different deviation. Thus we could jointly solve for the stress states consistent with the breakouts characteristics of both wells.

Implications

The Grauhnukar reinjection area is the location of the CarbFix carbon sequestration project, meaning the resulting stress data from this study may prove useful for the sequestration project (Gislason et al., 2010; Sigurdardottir et al., 2010). Reinjection into the new wells at Kolvidarholl-Husmuli started in late 2011, causing seismic activity that could be studied together with the data presented in this paper. No stress studies have been published directly related to the CarbFix project, but a link to this study could also be made regarding CO_2 sequestration.

The presence of seismic activity supports the critically stressed crust assumption and the presence of optimally oriented faults for slip within the given stress state. Current seismicity emphasizes the need for understanding the stress state for the CarbFix Carbon Sequestration project. BHTV data can provide this understanding and give more confidence to well and field stability. Pressure and temperature are the major factors discussed pertaining to the amount of carbon that can be sequestered (Gislason et al., 2010). With a 3D stress model, pressures can be simulated for the CarbFix wells for stability, and different wells will likely act differently when given the same amount of pressure because of the varying trajectories making stability questionable. BHTV could also be used to confirm carbon deposition along the wellbore wall if multiple logs were taken at time intervals before and after injection begins. This data could help plan future injection procedures and future drilling, should more wells be needed.

CONCLUSIONS

A preliminary stress state has been calculated for the Hellisheidi Geothermal Field using BHTV data from well HN-16. An iterative approach was implemented to minimize error from a lack of important input data, namely, a UCS for rocks encountered and an independent measurement of the S_{hmin} magnitude. The iterative approach had the following results:

a) S_{Hmax} azimuth is well constrained for UCS above 55 MPa, a reasonable assumption based on the cuttings log.
b) Stress magnitudes are not well constrained and require a better UCS model and direct measurement of the least compressive principal stress, S_{hmin}.
c) Stress field rotates from transitional strike slip-to-normal faulting to a normal faulting regime if a critically stressed crust is assumed, a reasonable assumption given recent seismic activity.

Three primary pieces of data will be sought out for future refinement of the model:

a) Rock samples for direct measurements of UCS and a calibration key for neutron porosity logs to calculate a porosity-to-UCS correlation.
b) A direct measurement of S_{hmin} magnitude in the form of a mini-hydrofracture test.
c) BHTV data in nearby wells with a distinctly different deviation.

ACKNOWLEDGEMENTS

The authors would like to thank Reykjavik Energy and ISOR for access to the data and approval to publish the results. Thank you also to The Fulbright Commission and the School for Renewable Energy Science for the original funding for this research and the Southern Methodist University Geothermal Laboratory for additional funds to continue work on this study.

REFERENCES

Angelier, J., Slunga, R.F., Bergerat, F., Stefansson, R., Homberg, C. (2004), "Perturbation of stress and oceanic rift extension across transform faults shown by earthquake focal mechanisms in Iceland," *Earth Planetary Science Letters* **219**, 271–284.

Angelier, J., Bergerat, F., Stefansson, R., Bellou, M. (2008), "Seismotectonics of a newly formed transform zone near a hotspot: Earthquake mechanisms and regional stress in the South Iceland Seismic Zone," *Tectonophysics*, **447**, 95-116.

Arnason, K., Karlsdottir, R., Eysteinsson, H., Flovenz, O.G., Gudlaugsson, S.Th. (2000), "The

resistivity structure of high-temperature geothermal systems in Iceland," *Proceedings of the WGC 2000, Japan*, 923-928.

Arnason, K., Eysteinsson, H., Hersir, G.P. (2010), "Joint 1D inversion of TEM and MT data and 3D inversion of MT data in the Hengill area SW-Iceland," *Geothermics*, **39**, 13-34.

Arngrimsson, H.O., and Gunnarsson, Th.B. (2009), *Tunneling in Acidic, Altered, and Sedimentary Rock in Iceland*. MS thesis, University of Iceland.

Blischke, A. (2011), personal communication, October 2010 through October 2011.

Björnsson, G. (2007), "Re-evaluation of the Hengill reservoir model and a simple evaluation of the productivity of new drilling areas," *Reykjavik Energy Report*, (in Icelandic) **3-2007**, 65.

Boettcher, M.S. and Marone, C. (2004), "Effects of normal stress variation on the strength and stability of Creeping Faults," *Journal of Geophysical Research*, **109**.

Boettcher, M.S., Hirth, G., and Evans, B. (2007), "Olivine friction at the base of oceanic seismogenic Zones", *Journal of Geophysical Research*, **112**.

Brace, W.F., Kohlstedt, D.L. (1980), "Limits on Lithospheric Stress Imposed by Laboratory Experiments," *Journal of Geophysical Research*, **85-B11**, 6248-6252.

Byerlee, J.D. (1978), "Friction of rocks," *Pure and Applied Geophysics*, **116**, 615-629.

Davatzes, N.C. and Hickman, S. (2009), "Fractures, stress and fluid flow prior to stimulation of well 27-15, Desert Peak, Nevada, EGS Project," *Proceedings 34th Workshop on Geothermal Reservoir Engineering*, Stanford University, Stanford, CA, SGP-TR-187.

Davatzes, N., and Hickman, S., (2010a), "Stress, fracture and fluid-flow analysis using acoustic and electrical image logs in hot fractured granites of the Coso Geothermal Field, California, U.S.A.," in M. Pöppelreiter, Garcia-Carballido and Kraaijveld (eds.), Dipmeter and Borehole Image Log Technology, *Amer. Assoc. Petroleum Geologists* **Memoir 92**, Tulsa OK, 259-294.

Davatzes N.C. and S. Hickman, (2010b). "The feedback between stress, faulting, and fluid flows: Lessons from the Coso Geothermal Field, CA, USA," *Proceedings of the World Geothermal Congress 2010*, Bali, Indonesia.

Davatzes, N.C. and Hickman, S. (2011), "Preliminary analysis of Fractures, Strength, and Stress Directions in the Newberry EGS well 55-29," *Geothermal Resources Council Annual Meeting*, **35**, San Diego, CA

Dziewonski, A., Ekstrom, G., Salganik, M. (1997), "Centroid-moment tensor solutions for July September 1996," *Physics of the Earth and Planetary Interiors*, **102**, 133-143.

Einarsson, P., Klein, F. W. and Bjornsson, S. (1977), "The Borgarfjordur Earthquakes of 1974 in West Iceland," *Bull. Seism. Soc. of Am.*, **67**, 187-208.

Foulger, G.R. (1988), "Hengill Triple Junction, SW Iceland: 2. Anomalous Earthquake Focal Mechanisms and Implications for Process within the Geothermal Reservoir and at Accretionary Plate Boundaries," *Journal of Geophysical Research*, **93**, 13507-13523.

Franzson, H., Gunnlaugsson, E., Arnason, K., Saemundsson, K., Steingrimsson, B., Hardarson, B. (2010), "The Hengill Geothermal System, Conceptual Model and Thermal Evolution," *Proceedings of the World Geothermal Congress 2010*, Bali, Indonesia.

Frolova, J., Ladygin, V., Franzson, H., Sigurdsson, O., Stefansson, V., Shustrov, V. (2005), "Petrophysical Properties of Fresh to Mildly Altered Hyaloclastite Tuffs," *Proceedings, World Geothermal Congress 2005*, Antalya, Turkey.

Garza-Cruz, T.V. and Davatzes, N.C. (2010), "Numerical modeling of the Nucleation conditions of Petal-Centerline Fractures below a Borehole floor, a Sensitivity Study and Application to the Coso Geothermal Field," *Geothermal Resources Council Transactions*, **34**, San Francisco, California.

Gislason, S.R., Wolff-Boenisch, D., Stefansson, A., Oelkers, E.H., Gunnlaugsson, E., Sigurdardottir, H., Sigfusson, B., Broecker, W.S., Matter, J.M., Stute, M., Axelsson, G., Fridiksson, T. (2010), "Mineral Sequestration of carbon dioxide in basalt: a pre-injection overview of the Carbfix Project," *International Journal of Greenhouse Gas Control*, **4**, 537-545.

Gudfinnsson, G.H., Helgadottir, H.M., Feucht, C., Ingolfsson, H. (2010), "Husmuli – Hola HN-16," *Iceland Geosurvey*, (in Icelandic), **ISOR-2010/069**.

Haimson, B.C., Voight, B., (1977), "Crustral stress in Iceland," *Pure Applied Geophysics*, **115**, 153-190.

Haimson, B.C., (1979), "New stress measurements in Iceland reinforce previous hydrofracturing results, SHmax is perpendicular to the axial rift zones," *EOS*, **60**, 377.

Haimson, B.C., Rummel, F., (1982), "Hydrofracturing Stress Measurements in the Iceland Research Drilling Project Drill Hole at Reydarfjordur, Iceland," *Journal of Geophysical Research*, **87**, 6631-3349.

Hardarson, B.S., Einarsson, G.M., Kristjansson, B.R., Gunnarsson, G., Helgadottir, H.M., Franzson, H., Arnason, H., Águstsson, K., and

Gunnlaugsson, K. (2010), "Geothermal Reinjection at the Hengill Triple Junction, SW Iceland," *Proceedings of the World Geothermal Congress 2010*, Bali, Indonesia.

Hast, N. (1969), "The state of stress in the upper part of the Earth`s crust," *Tectonophysics*, **8**, 169-211.

Hearst, J.R., Nelson, P.H., Paillett, F.L. (2000), Well logging for physical properties: A handbook for geo-physicists, geologists and engineers, 2nd ed.: New York, *John Wiley & Sons*, 483 p.

Heffer, K.J., Fox, R.J., McGill, C.A., and Koutsabeloulis, N.C. (1995), "Novel Techniques Show Links between Reservoir Flow Directionality, Earth Stress, Fault Structure and Geomechanical Changes in Mature Waterfloods," *SPE Annual Technical Conference and Exhibition, Dallas TX*, 22-25 October, 1995, SPE paper 30711.

Heffer, K. (2002), "Geomechanical Influences in Water Injection Projects: An Overview," *Oil and Gas Science and Technology*, **57-5**, 415-422.

Heidbach, O., Tingay, M., Barth, A., Reinecker, J., Kurfeß, D., and Müller, B. (2008), "The World Stress Map database release 2008," doi:10.1594/GFZ.WSM.Rel2008.

Hickman, S., and N.C. Davatzes, (2010). "In-situ stress and fracture characterization for planning of an EGS stimulation in the Desert Peak geothermal field, NV," *Proceedings, 35th Workshop on Geothermal Reservoir Engineering*, Stanford University, Stanford, CA, SGP-TR-188.

Jaeger, J.C., and N.G.W. Cook, (1979). Fundamentals of rock mechanics, 2nd ed.: New York, *Chapman and Hall*, 585 p.

Khodayar, M., Bjornsson, S. (2010), "Surface Deformation of May 29, 2008 earthquake near Hveragerdi, South Iceland Seismic Zone and Hengill geothermal area," *Iceland Geosurvey*, **ISOR-2010/033**.

Klein, F. W., Einarsson, P. and Wyss, M. (1977), "The Reykjanes Peninsula, Iceland, earthquake swarm of September 1972 and its tectonic significance," *Journal of Geophysical Research*, **82**, 865-888.

Li, L. and Aubertin, M. (2003). "A general relationship between porosity and uniaxial strength of engineering materials," *Canadian Journal of Civil Engineering*, **30**, 644-658.

Lund, B. & Slunga, R. (1999), "Stress tensor inversion using detailed microearthquake information and stability constraints: application to Olfus in southwest Iceland," *Journal of Geophysical Research*, **104,** 14947–14964.

Lund, B. and Townend, J. (2007), "Calculating horizontal stress orientations with full or partial knowledge of the tectonic stress tensor," *Geophysical Journal International*, **170**, 1328-1335.

Miller, A.D., Julian, B.R., and Foulger, G.R., (1998), "Three-dimensional seismic structure and moment tensor of non-double-couple earthquakes at the Hengill-Grensdalur volcanic complex, Iceland," *Geophysical Journal International*, **133**, 309-325.

Moos, D. and Pezard, A.P. (1996), "Relationship between strength and physical properties of samples recovered during legs 137, 140, and 148 from hole 504B," Alt, J.C, Kinoshita, H., Stokking, L.B., Michael, P.J. (Eds.), *Proceedings of the Ocean Drilling Program, Scientific Results*, **148**, 401-407.

Nielsson S., and Franzson, H. (2010), "Geology and hydrothermal alteration of the Hverahlíð HT-system, SW-Iceland." *Proceedings of the World Geothermal Congress*, Bali, Indonesia.

Peska, P., and M.D. Zoback, (1995), "Compressive and tensile failure of inclined wellbores and determination of in situ stress and rock strength," *Journal of Geophysical Research*, **100-B7**, 12791–12811.

Price, R.H., R.J. Martin III, and P.J. Boyd, (1993), "Characteriztion of porosity in support of mechanical property analysis," SAND—92-2153C, 15 p.

Rahman, M.K., Hossain, M.M., and Rahman, S.S. (2002), "A shear-dilation-based model for evaluation of hydraulically stimulated naturally fractured reservoirs", *International Journal for Numerical and Analytical Methods in Geomechanics*, **26**, 469-497.

Saemundsson, K. (1995a), "Hengill. Geological map (bedrock)," *Iceland Geosurvey*, 1:5000.

Saemundsson, K. (1995b), "Hengill. Map of thermal activity, alteration and hydrology," *Iceland Geosurvey*, 1:25000.

Schindler, M., Nami, P., Schellschmidt, R., Teza, D., and Tischner, T. (2008), "Summary of hydraulic stimulation operations in the 5-km-deep crystalline HDR/EGS reservoir at Soultz-sous-Forêts, *Proceedings, 33rd Workshop on Geothermal Reservoir Engineering*, Stanford University, Stanford CA, SGP-TR-185

Schön, J.H. (1996), Handbook of Geophysical Exploration: Volume 18: Seismic Exploration, Physical Properties of Rock; Helbig, K. and S. Treitel (eds.) *Elsevier*, Amsterdam, **18**, 583p.

Sigurdardottir, H. (2010), "CarbFix - CO_2 Fixation into Basalts, Hellisheidi, Iceland Annual Status Report 2010," *CarbFix Project*.

Sykes, L. R. (1967), "Mechanism of earthquakes and nature of faulting on the mid-oceanic ridges," *Journal of Geophysical Research*, **72**, 2131.

Valley, B., and Evans, K.F. (2007), "Stress state at Soultz-sous-Forêts to 5 km depth from wellbore failure and hydraulic observations," *Proceedings, 32nd Workshop on Geothermal Reservoir Engineering*, Stanford University, Stanford CA, SGP-TR-183.

Willis-Richards, J., Watanabe, K., and Takahashi, H. (1996), "Progress toward a stochastic rock mechanics model of engineered geothermal systems," *Journal of Geophysical Research*, **101**, 17481-17469.

Zoback, M. D., C. A. Barton, M. Brudy, D. A. Castillo, T. Finkbeiner, B. R. Grollimund, D. B. Moos, P. Peska, C. D. Ward, and D. J. Wiprut, (2003), "Determination of stress orientation and magnitude in deep wells," *International Journal of Rock Mechanics and Mining Sciences*, **40**, 1049 – 1076, doi:10.1016/j.ijrmms.2003.07.001.